

Observations of the daytime boundary layer in deep alpine valleys

C. Chemel* and J. -P. Chollet

Laboratoire des Écoulements Géophysiques et Industriels

Université Joseph Fourier – C.N.R.S. – I.N.P. Grenoble

BP 53, 38041 Grenoble, Cedex 9, France

Abstract. Mixing depth structure and its evolution have been diagnosed from radar wind profiler data in the Chamonix and the Maurienne valleys (France) during summer 2003. The behaviour of refractive index structure parameter C_n^2 peaks coupled with the vertical air velocity variance σ_w^2 was used to locate the height of the mixed layer. Tethersonde vertical profiles were carried out to investigate the lower layers of the atmosphere in the range of approximately 400-500 m above ground level. The tethersonde device was especially useful to study the reversal of the valley wind system during the morning transition period. Specific features such as wind reversal and convective mixed layer up to approximately the altitude of the surrounding mountains were documented. The wind reversal was observed to be much more sudden in the Maurienne valley than in the Chamonix valley.

Keywords: Air pollution, Convective boundary layer, Deep valleys, Tethered balloon, UHF radar wind profiler.

* Corresponding author: e-mail: Charles.Chemel@hmg.inpg.fr



1. Introduction

Alpine valleys are particularly sensitive to air pollution due to emission sources generally concentrated near the valley floor and local meteorology induced by complex terrain. The program POVA ('Pollution des Vallées Alpines'), a multiagency collaboration was launched in 2000 (Jaffrezo et al., 2005). The main objectives of the POVA program are to characterize the pollution sources and study the relationships between atmospheric dynamics and pollution events in the Chamonix and the Maurienne valleys (France). The program includes several intensive observation periods (IOPs) associated with modelling. The last IOPs took place in the Maurienne valley from June 25 to July 2, 2003 and in the Chamonix valley from July 4 to July 11, 2003. Numerous measurements of pollutant concentrations such as ozone (O_3), nitric oxide (NO), nitrogen dioxide (NO_2), sulfur dioxide (SO_2), carbon monoxide (CO) and particles were performed. In particular, field campaigns have investigated the mountain-valley wind system in both valleys. Investigations of small-scale flow fields were carried out and aimed at detailing the lower layers of the atmosphere.

Valley wind system and mixing depth evolutions are assumed to be key processes of the pollution in deep valleys. Diagnosing the convective boundary layer (CBL) structure and its evolution is decisive for under-

standing the dispersion and transport of pollutants such as O_3 and its precursors. The main objective of this study aims at depicting the local mixed layer structure and its evolution in the Chamonix and the Maurienne valleys. Special emphasis was put on the morning transition period to give a better understanding of the formation of the CBL.

2. Determination of the mixing depth

2.1. PREVIOUS WORK

Dynamical issues in mountainous areas have been discussed in numerous studies. Thermally driven winds in wide valleys have already been well documented. Whiteman (1990) gave an overview of knowledge on the meteorological aspects. Stewart et al. (2002) have described thermally driven wind systems in four regions of the U.S. Intermountain West using a large surface data set. A stable nocturnal boundary layer (NBL) forms at the surface at night when air temperature near the ground decreases in response to the radiational cooling of the surface. This process produces a shallow inversion and stable conditions, which reduce vertical mixing, thus confining surface-based pollutants to the lowest few hundred meters. Starting shortly after sunrise, the convec-

tive boundary layer develops from the valley floor and slopes on the mountain sides during the day because of ground surface heating. This process generates thermal structures which vertically mix heat, moisture, momentum, and pollutants. Thermally-generated upslope flows carry pollutants along the slopes up to higher altitude and may dilute them at larger scale. The entrainment zone at the top of the mixed layer is characterized by a stable temperature lapse rate that limits the entrainment of air from the free atmosphere.

Seibert et al. (2000) gave an extended review of operational methods for the determination of the mixing depth. Intercomparison studies of the CBL depth determination from different measurement systems have been performed by Coulter (1979), Kaimal et al. (1982), Marsik et al. (1995) and Seibert et al. (2000). Relative differences derived from these studies are typically less than 10 % if the inversion capping the CBL is well defined. Generally, many practical techniques used to estimate the height of the mixing layer involve determining the vertical static stability structure for a particular sounding profile (Coulter, 1979; Heffter, 1980), therefore classifying where air is unstable, stable or neutral within the profile.

Coulter (1979) described a method for estimating daytime mixing depths using the local static procedure. He defined it as the altitude, above the surface layer, at which the potential temperature gradient

$\partial\theta/\partial z$ first became greater than zero, where θ is the potential temperature and z is the vertical coordinate. The Heffter's (1980) technique consists of analysing θ vertical profiles in order to locate a possible inversion, which is assumed to mark the top of the mixed layer. It is defined as the lowest inversion whose potential temperature lapse rate is equal to or larger than 5 K km^{-1} , and the temperature difference between the inversion base and its top must exceed 2 K (Piringer et al., 1998).

Using non-local static stability methods to estimate the mixed layer depth is often preferred over traditional techniques as they incorporate convective parcel movements (Stull, 1991). These methods involve displacing parcels of virtual potential temperature θ_v upward from the relative maxima and downward from the relative minima. Parcel movement is based on buoyancy measured by comparing the virtual potential temperature of the parcel to the environment at the same height. Ascent or descent of the parcel is tracked until it intersects the surrounding profile or becomes neutrally buoyant. Once all parcel movements have been tracked along the whole vertical profile, the static stability is then determined for each portion of the sounding domain. As an example, a tethered sonde vertical virtual potential temperature profile from *Les Praz de Chamonix* site in the Chamonix valley starting at 0617 UTC on July 8, 2003 is displayed in Figure 1. Stull's (1991)

analysis of non-local static stability enables us to detect stable layers around 100 – 150 m and 200 – 250 m above ground level (a.g.l.).

Figure 1

Mathematical methods based on conceptual models may also be used to determine the capping inversion of the CBL. Rampanelli and Zardi (2004) described a simple algorithm by means of best-fit analysis of soundings with a smooth ideal profile. This method assumes a constant-potential-temperature mixed layer, a strongly stratified entrainment layer and a constant-lapse-rate free atmosphere.

Remote sensing techniques provide alternative methods to estimate the mixing depth. Radar wind profilers utilize microwave pulsed signals to vertically probe the atmosphere. The return patterns from these signals permit one to measure vertical profiles of horizontal wind speed and direction. The data can also be used to depict the temporal evolution of the mixing depth (Marsik et al., 1995). In fair weather conditions, the boundary layer is often more humid than the free atmosphere allowing an interpretable boundary or interface to be present in the return signal. This signal pattern is then often used to estimate the height of the mixed layer. Signals should be assessed with care as ground clutter such as buildings, insects, and vegetation can create interpretation problems (Marsik et al., 1995). Further, the existence of clouds and precipitation can often affect return signal patterns due to additional pulse scattering that is difficult to examine (Fairfall, 1991).

2.2. APPROACH

During the POVA IOPs, the structure of the CBL was described using a UHF radar wind profiler. Beside providing winds, the radar wind profiler also measured reflectivity, which can be used to compute the refractive index structure parameter C_n^2 . This parameter measures fluctuations in the refractive index of the atmosphere. It is directly proportional to the range-corrected signal-to-noise ratio (SNR) of the backscattered power (Ottersten, 1969). C_n^2 peaks often occur where vertical gradients of θ_v and mixing ratio r have their maximum values. Due to small-scale buoyancy fluctuations associated with the entrainment process, the C_n^2 can be a very useful parameter for estimating the CBL depth. Different C_n^2 -based techniques have been investigated. Angevine et al. (1994) estimated CBL depth in clear air using SNR peaks. Heo et al. (2003) have developed a method using both C_n^2 peaks and vertical air velocity variance σ_w^2 . This method is able to discriminate between peaks due to the top of the mixed layer and peaks due to a cloud layer or a residual layer.

The turbulent kinetic energy dissipation rate ϵ retrieval from spectral width measurements provides additional information coupled with reflectivity data. Jacoby-Koaly et al. (2002) gave an excellent overview of methods for ϵ determination. The turbulent dissipation rate is bal-

anced by the buoyancy flux in the mixed layer away from the boundary and decreases rapidly once above.

Due to ground clutter and atmospheric echoes, radar wind profilers are often blind close to the ground surface (in the range of 0-200 m a.g.l.). Furthermore, measurements have a limited vertical resolution (normally 50-250 m). For a reliable prediction of chemical species concentrations, an accurate description of the mixing depth evolution during the morning and evening transition periods is essential. Few observational studies addressed this issue in valley flows. Clements et al. (1989) investigated the mean properties of the nocturnal drainage flow down a valley using an instrumented tethered balloon and observed a strong down-valley flow near the valley floor and a reversed up-valley flow aloft. Whiteman (1982), Müller and Whiteman (1988) and Helmis et al. (1990) looked into upward growth of the CBL during the morning transition in deep mountain valleys. The NBL development in valleys has been described in previous studies by Whiteman (1986) and Doran et al. (1990). It is produced by the convergence of cold downslope flows over the valley center, and the subsequent buildup of a cold air layer within the valley. During the POVA field campaigns in summer 2003, the lower layers of the atmosphere were documented using a tethered balloon. Combined with the radar wind profiler, the tethered balloon provided full vertical profiles. The tethered balloon device enabled us to

choose the ascent velocity according to the desired vertical resolution and was equipped with a trace gas concentration measuring system. Operations were allowed to be more continuous in time than common radiosoundings which could provide only ‘snapshot’-like profiles.

3. Observational site

The present study refers to a fraction of the French alpine region. The topography of the region (see Figure 2) is composed of several valleys which differ in cross-section shape, length and orientation. Even if the most frequent synoptic regimes are southeastward to northeastward, the assessment of the air flow is especially challenging because of the effects of synoptic-scale interactions on valley-scale circulations. The Chamonix valley (site **A**) runs from southwest to northeast for about 15 km and is over 2000-m deep on average. The altitude of the highest mountain of the southeast mountain ridge (Mont-Blanc) is 4810 m above mean sea level (a.m.s.l.) The peak-to-peak distance is around 4 km and the width of the valley bottom is about 1.5 km. The Maurienne valley (site **B**) is five times as long as the Chamonix valley. The length of this curve-shaped valley is approximately 80 km. The mountain ridges on both sides reach altitudes of around 3000 m a.m.s.l. and the valley

bottom is about 2-km wide. Both valleys have slopes up to 40° – 50° on the mountain sides, and have a valley floor that falls in the range of 13–14 m per km.

Figure 2

Observational sites are indicated by dark gray dots in Figure 2. The radar wind profiler was situated at *Le Clos de l'Ours* in the Chamonix valley and *Modane* in the Maurienne valley. *Le Clos de l'Ours* site is located on the valley floor at an altitude of 1040 m a.m.s.l. *Modane* site is located close to the center of the Maurienne valley at an altitude of 1090 m a.m.s.l. Both sites are representative of the bottom of the valleys and measurements may be extrapolated to the main valley axes. In the Chamonix valley, tethered balloon and radar wind profiler sites were spaced out 1.5 km apart whereas they were in the same place in the Maurienne valley. *Les Praz de Chamonix* site was selected in the Chamonix valley owing to its quite broad expanse to operate the tethered balloon. Experiments were conducted in suburban area of small towns (local populations lower than 10,000 inhabitants) in both valleys.

Several other measurements are available from IOPs. Both valleys were equipped with a network of ground monitoring stations including measurements of pollutant concentrations and meteorological variables. Jaffrezo et al. (2005) provided a detailed presentation of the data set obtained during IOPs.

4. Experiment and method

4.1. EQUIPMENT AND COLLECTION OF DATA

The mobile radar wind profiler used in the POVA experiment is a ‘clean-air’ three panel 1238 MHz UHF Doppler radar system designed and operated by Degreane Horizon to provide wind speed and direction 24 h a day under all weather conditions. ‘Clean air’ radars detect irregularities in backscattered signals due to refractive index inhomogeneities caused by turbulence (Ottersten, 1969). In the lower troposphere these inhomogeneities are mainly produced by humidity fluctuations. The operational mode sampled continuously the boundary layer from 80 m to 3500 m a.g.l. along the vertical, using a 80-m resolution and a 6-min acquisition cycle. Characteristics of the UHF radar wind profiler used in the POVA experiment are reported in Table I. The first three moments were computed with the weighted contiguous spectral lines selected during the last 30 min. The 30-min consensus performs a temporal filter over the considered period removing or smoothing out spurious unwanted echoes.

Table I

A tethered balloon data collection system was used to provide experimental data close to the ground surface. Vertical sounding operations at each site consisted of the deployment of a Tethersonde Meteor-

logical Tower System (TMT)TM by Vaisala Inc. with an electrochemical concentration cell ozone sonde (Model 4Z ECC-O₃-Sonde)TM by EN-SCI Corporation beneath a 5-m³ helium-filled balloon. Soundings of meteorological variables and O₃ were conducted approximately up to 400-500 m a.g.l. Measurements were averaged using a sliding window with a 20-meter resolution. There were no systematic differences between the ascending and descending soundings. Thus, vertical displacements of the tethered balloon were assumed to have no significant influence on the measurement of the variables. Operations were restricted to daylight hours to meet aircraft safety considerations. Tethersonde flights were halted from midday to early evening due to strong up-valley winds.

Data were collected from June 25 through July 11, 2003. Short precipitation events occurred, preventing some tethered balloon data from being collected and affecting the quality of the radar wind profiler signal. The whole week of radar wind profiler measurements in the Chamonix valley has been reported by Brulfert et al. (2005a). The present study focuses on July 8 in the Chamonix valley and June 29 in the Maurienne valley. The meteorological conditions during the two studied episodes favoured high ozone concentrations as high-pressure systems located over the area produced clear skies, weak winds, hot temperatures and a subsidence inversion. Ozone concentrations peaked beyond 80 ppbv on both periods in surrounding cities.

4.2. MIXING DEPTH EVALUATION

The mixing depth definition adopted by Seibert et al. (2000) and referred as mixing height has been retained for this work: “*The mixing height is the height of the layer adjacent to the ground over which pollutants or any constituents emitted within this layer or entrained into it become vertically dispersed by convection or mechanical turbulence within a time scale of about an hour.*”

Hourly mixing depths were estimated from C_n^2 data during the day using an algorithm proposed by Heo et al. (2003). C_n^2 data were combined with σ_w^2 to monitor the growth of the CBL. Assuming that heat flux decreases linearly with height from the ground surface to the top of the CBL in a dry convective mixed layer, this method consists in determining the ‘zero flux level’. The heat flux is proportional to the standard deviation of the vertical velocity σ_w (Weill et al., 1980)

$$\frac{\sigma_w^3}{z} \approx \alpha^{3/2} \frac{g}{\theta} \overline{w'\theta'_v},$$

where α a universal constant ($\alpha = 1.4$). The term $(g/\theta) \overline{w'\theta'_v}$ represents a local buoyant production of turbulent kinetic energy, where g , w' and θ'_v are the gravitational acceleration, vertical velocity and virtual potential temperature fluctuations, respectively. Then, the mixing depth corresponds to the peak of C_n^2 close to the ‘zero flux level’, which is

obtained by an extrapolation to zero of the linear regression of the σ_w^3/z profile.

Other techniques were used to provide further informations. Day-time turbulent kinetic energy dissipation rate ϵ is almost constant across the whole mixing layer (Caughey et al., 1979). Above the CBL top, the turbulent dissipation rate rapidly decreases to near zero. ϵ vertical evolution was used to get a better estimate of the mixing depth coupled with information derived from reflectivity data. During the morning and evening transition periods, wind, θ and O_3 profiles from tethered sonde measurements complement the radar wind profiler data.

5. Experimental results

5.1. CHAMONIX VALLEY – JULY 8, 2003

5.1.1. *Flow structure*

The sounding launched on July 8, 2003 at 1200 UTC in Lyon 100-km west of the Chamonix valley showed a large dew point temperature gradient between the surface and the top of the planetary boundary layer at roughly 825 hPa (about 2000 m). The prevailing synoptic wind blows south-southeastward.

Figure 3a illustrates the diurnal changes in the mixed layer structure on July 8, 2003. The upper limit of the mixed layer is plotted as white dots from C_n^2 peaks. All the pronounced C_n^2 peaks are located above the level where σ_w^3/z goes to zero. Therefore the mixing depth is determined by the lowest height of the C_n^2 peaks. During the transition periods, the mixing depth is estimated by analysing tethersonde data with Stull's (1991) technique and reported as two black stars in Figure 3a. At night, the strong stability of the NBL confines vertical mixing of momentum and surface-based pollutants to a shallow layer (i.e., 100-m to 200-m thick) near the ground. After daybreak (0700 UTC), the ground surface warms up, resulting in the growth of the CBL. The CBL grows up to an afternoon depth of about 1700 m a.g.l. The spread of the large C_n^2 values during daylight hours is likely to be due to the strong convective activity. The evolution of C_n^2 is in good agreement with the ϵ evolution. Figure 3b emphasizes the strong turbulent activity in the CBL. By early evening (1900 UTC), stable conditions associated with the NBL form.

Figure 3

During the transition periods, tethersonde profiles are particularly useful to depict the boundary layer structure and its evolution. Figure 4 shows wind structure pattern evolution from tethered balloon ascents and descents for July 8, 2003. Soundings show the reversal of the valley wind system during the transition periods. Wind direction reverses from down- (50°) to up- (230°) valley in the morning (0700 UTC) and

the opposite at night (1900 UTC). Wind speed is maximum when being up-valley and peaks at $5 - 6 \text{ m s}^{-1}$ at 1000 UTC.

Figure 4

Changes in wind regime gradually proceed from the ground to upper layers. Observation of the lower layers of the atmosphere corroborates the observation from the radar wind profiler up to about 400-500 m a.g.l. Figures 5a and 5b show time-height cross sections of horizontal wind speed and direction, respectively, obtained from the first moment of the Doppler spectrum for July 8, 2003.

Figure 5

Sequences of θ soundings are presented in Figure 6. No Radio Acoustic Sounding System (RASS) data were available to extend these profiles. However successive downward displacements of the potential temperature curve after sunrise are consistent with the destruction of the inversion by subsidence (Whiteman, 1982).

Figure 6

During the strong convective activity period, a superadiabatic layer is observed near the ground surface that implies a strong vertical mixing. However multiple superadiabatic layers are found throughout the profiles as soon as the morning transition period starts. The cross section of the valley in Figure 7 suggests that the underlying physical mechanism is the detachment of turbulent structures from the narrow pass towards downtown *Chamonix*. Nevertheless the signal is not very clear since a critical level is located at the height of the pass (about 400 m a.g.l.), which is close to the upper limit of profiles.

There are essentially two types of turbulence in the CBL: mechanical due to the instability of the vertical wind shear and thermal due to the buoyancy forces in the atmosphere. The combination of wind and temperature stratification is a complex mixture that makes the characterization of the generation and nature of these small potential temperature deformations difficult.

Figure 7

To assess the origin of the structures present throughout profiles an analogy with hydraulics is used. The flow pattern over an obstacle reveals a range of regimes dependent on the Froude number Fr , here defined as the competition between inertial and buoyant forces

$$Fr^2 = \frac{U^2/h}{g \Delta\theta/\Theta_0},$$

where U is the upstream mean velocity, h is the local depth of the flow, $\Delta\theta$ is a typical temperature disturbance and Θ_0 is the large-scale potential temperature. The pass in Figure 7 represents an obstacle which is about 400-m high. A rough estimation of the upstream mean velocity may be 2 m s^{-1} . At night the stability of the NBL inhibits vertical structure development. After daybreak the descending flow from the pass constrains the flow response to occur within a capped inversion layer in the order of 100-m thick. Assuming that the atmosphere is stable ($\Delta\theta = 1 \text{ K}$), this yields to $Fr = 1.1$ using $\Theta_0 = 303 \text{ K}$. At the tethered balloon location the wind speed is as low as 1 m s^{-1} .

The capping inversion is eroded and the depth of the flow corresponds nearly to the pass height. The stratification is slightly stable ($\Delta\theta = 0.5$ K) and the derived Froude number is equal to 0.4 using $\Theta_0 = 303$ K. Therefore downwind of the pass there can be a hydraulic jump leading to the detachment of turbulent structures towards the tethered balloon.

Interpreting order of magnitude analysis is not straightforward and the observed shallow superadiabatic layers are also likely to be due to the interaction between the rising CBL and the stable core aloft which is not completely eroded by the convective activity. The wind reversal induces small structures which produce temperature fluctuations. This shifting process seems to be hindered by the *Mer de Glace* glacier (referred as *tributary* in Figure 7) located southeastward between the tethered balloon site and the narrow pass. Convergence effects may intensify the stable descending flow.

5.1.2. *Diurnal evolution*

When looking at the ozone measurements in Figure 8, several features that are important for understanding the role that mixing depth plays in the air quality of this region can be described.

Figure 8

After daybreak (0700 UTC) ground surface heating triggers the development of the CBL, but further vertical growth is inhibited by the subsidence inversion. This subsidence warming mechanism was first

noted by Whiteman and McKee (1982) in several deep mountain valleys in Colorado, USA. The temperature inversion develops aloft as a result of air gradually sinking over the valley area and being warmed by adiabatic compression. The strong ozone concentration gradient early in the morning weakens at later times until there is almost uniform mixing in the vertical. Ozone increases to a background level of 70–75 ppbv, which is characteristic of the free atmosphere and is vertically mixed down to the ground. Therefore ozone is observed to be a good tracer of mixing properties of the flow field. The boundary layer over such a complex terrain is shown characteristically disturbed as illustrated by θ profiles in Figure 6. The evening transition period begins shortly before sunset, as convective thermals decrease and can no longer drive the mixed layer. As the ground surface cools down, a surface-based temperature inversion develops producing the NBL, which is shown to be less than 100-m deep by sunrise. The region between the NBL and the former capping inversion height is the residual layer (RL). Ozone or ozone precursors mixed upwards in the CBL during daytime likely remain in the RL, and the strong stability associated with the NBL ‘shielded’ these pollutants aloft from the titrating effects of fresh NO emissions near the ground surface.

5.1.3. *Growth rates*

The relatively slow growth rate of the mixing depth in Figure 8 likely confines emissions of nitrogen oxides and volatile organic compounds near the ground surface for a longer time, and thus photochemistry is activated in the presence of high precursor concentrations. The origin of anthropogenic pollution sources in the area is mainly due to traffic (66 %) and economic activities (14 %) according to the POVA emission inventory of the valley. The methodology to draw up the emission inventory is similar to the Maurienne valley one (Brulfert et al., 2005b). This slow growth rate is perhaps one key factor in the weak ozone production in the morning within the valley in summer. Differences of solar exposure across the valley are maximized during the morning and evening transition periods. Differential solar heating might cause the mixing layer over slopes facing the south to be higher during morning and lower during early evening. Upslope flows established during the convective activity period enhance the vertical development of the CBL. Mixing depth over edges of the valley can be lifted relative to mixing depths at the bottom of the valley. Air to replace that removed by slope flows could come from valley winds and need not involve a counter recirculation of pollutants at all. Then pollutants carried along the slopes may be diluted at higher altitude.

5.1.4. *Descending inversion*

Another important factor for understanding air quality is the descending subsidence inversion observed from the early evening (1730 UTC). The mixing depth decreases slowly and regularly, implying a continuous stable layer above the NBL. The descending inversion reduced the vertical extent of mixing, which results in a weaker dilution of ozone and its precursors. As photochemical production of O₃ persists in late afternoon and stops in the evening, O₃ concentration measured near the ground surface typically decreases as a result of deposition and titration by NO. Nevertheless a weak increase in ground O₃ concentration is observed at night. Figure 9a shows a fast rise of 15 ppbv from 2200 UTC to 2300 UTC in *Le Clos de l'Ours* ground monitoring station located close to the center of the Chamonix valley. It cannot be caused by chemical processes. The top of the RL, formerly the daytime capping inversion, may combine with the NBL or participate in turbulent episodes of mixing in the NBL. The increase might be caused by downward mixing resulted from turbulence produced by a low-level jet (Corsmeier et al., 1997). However no strong wind velocity is observed at night. Such an increase is presumed to be due to the transport of ozone-rich air mass from higher altitude by down-valley winds. It should be cautioned that more polluted air at higher elevations is entrained in the down-valley flow, thus mixing air and increasing O₃ concentration. The ratio of

NO_x (the sum of nitrogen oxides $\text{NO} + \text{NO}_2$) to NO_y (the sum of all odd-nitrogen species $\text{NO}_x + \text{PAN} + \text{HNO}_3$) can be used to estimate the ‘chemical age’ of the air mass (Banta et al., 1997). A high ratio (greater than 0.9) implies that NO_y is mostly composed of NO_x ($\text{NO}_y \equiv \text{NO}_x$). Therefore the air mass contains fresh pollution. Low values (less than or equal to 0.6) suggest that most of the NO_x has already been transformed to stable end species and the air mass is chemically aged. Figure 9b shows that NO_x/NO_y ratio drops below 0.6 for this particular episode in *Argentière* ground monitoring station located upstream of the narrow pass. This strengthens that the increase in O_3 concentration is most likely associated with aged polluted air from an elevated layer descending from the narrow pass or the *Mer de Glace* glacier.

Figure 9

5.2. MAURIENNE VALLEY – JUNE 29, 2003

The prevailing winds came from the sector between west and south, with partly cloudy weather during the morning on June 29, 2003.

The wind regime changes suddenly across the whole boundary layer instead of gradually proceeding from ground to upper layers as observed in the Chamonix valley. Figure 10 suggests that the wind reverses from down to up-valley in only two couples of ascent and descent. The morning transition period lasts about 30 min to be compared to

more than 2 h in the upper end of the Chamonix valley. In addition winds are stronger in the morning in the Maurienne valley than in the Chamonix valley. The mean velocity is around 5 m s^{-1} except during the transition period with lower values. Wind reversal is observed in the morning at 0800 UTC and in the evening at 1900 UTC with the same behavior on every sunny day of the IOP week.

Figure 10

Profiles of meteorological parameters and ozone concentration measured in the Maurienne valley are smoother than in the Chamonix valley. The detailed description of the CBL evolution is similar in both valleys (see sections 5.1.2 to 5.1.4).

The temporal evolution of surface wind vectors can be detailed in hodographs. 24-h hodographs reveal the daily variation of both wind speed and direction. The hodograph in Figure 11a plotted in *Modane* ground monitoring station on June 29, 2003 shows that most of the time wind is aligned along the valley axis. It may be regarded as an ellipse with eccentricity defining its shape. The eccentricity goes to 1 and suggests that wind reversal is very sudden. It may be compared to the hodograph in Figure 11b plotted in *Argentière* ground monitoring station in the Chamonix valley with a much wider loop (ellipse with eccentricity 0.85). This wider loop may be attributed to slope winds and a more complex topography likely to develop transversal circulation during the transition periods.

Figure 11

One possible explanation for the differences observed between these two valleys lies in the different valley lengths and geometries. Müller and Whiteman (1988) defined a topographic amplification factor (TAF) to characterize a valley geometry. This geometrical parameter can be used to interpret the thermal energy budget within a valley using the first law of thermodynamics. A given input (or extraction) of thermal energy to (or from) a volume of air will change its temperature. The smaller the volume, the larger the temperature changes for a fixed energy increment. The TAF is the valley drainage area to volume ratio divided by the plain drainage area to volume ratio. Hence it can be written as

$$\text{TAF}(z) = \frac{A_v/V_v}{A_p/V_p},$$

where A is the drainage area, V is the volume of air and the subscripts v and p stand for valley and plain, respectively. For a very flat valley, the TAF goes to 1 and for a steep and deep valley, a TAF greater than 2 is the rule. TAF is generally estimated using valley cross sections by assuming a uniform cross section area along the valley axis (Sakiyama, 1990). This assumption produces poor estimations of TAF for valleys that have complex shapes of cross sections along their axes. Thus, both valleys were cut out in representative parts. TAFs were computed for each part of both valleys and over the entire valley areas. Figure 12 illustrates the chosen sub-areas in both valleys. The results are plotted

in Figure 13 as a function of nondimensional height z/z_{Top} , where z_{Top} is the maximum height of the topography. The average TAF for the Chamonix and the Maurienne valley length over the valley depth is found to be 1.84 and 2.35, respectively. These values vary slightly with height and indicate the broadly V-shaped profile for the Chamonix valley and the predominantly convex shaped profile in the Maurienne valley. Therefore one would expect that temperature changes in the Maurienne valley will be larger than in the Chamonix valley. Consequently the inversion breakup will be faster in the Maurienne valley with the same input of thermal energy.

Figure 12

Figure 13

The TAF in the Maurienne valley is smaller close to the mouth of the valley than in the upper valley end where the terrain is somewhat more open. The funnelled wind flow may be accelerated when being up-valley leading to a much more sudden wind reversal.

6. Discussion and conclusions

Radar wind profiler and tethered balloon were operated to probe the vertical structure of the atmosphere and its evolution during the POVA field campaigns in summer 2003. Wind reversal and mixing depth evolution were carefully documented using radar wind profiler and

tethered balloon data. The maximum backscatter intensity method coupled with the determination of the vertical velocity variance σ_w^2 correctly estimated the mixing depth when vertical mixing owing to solar heating was significant and the vertical gradient of both θ_v and r in the entrainment zone was strong enough. The tethered sonde device was especially useful to study the reversal of the valley wind system during the morning transition since proceeding from the ground surface to upper layers. One of the goals of this study was to document full vertical profiles joining up a tethered balloon with a radar wind profiler. Operating both measurement devices in the same place made possible to document the vertical direction from the ground up to about 3000 m. The results presented above provide a qualitative and quantitative description of the valley wind system and mixing depth.

To conclude this study, a number of our initial questions are now addressed as follows:

- What are the characteristics of the thermally driven and synoptic-scale flows inside and above both valleys?

At least during these summer field campaigns, both valleys exhibit similar behavior with a wind reversal twice a day and a mixed layer up to approximately the altitude of the surrounding mountains. Hodographs are proposed as a characterization of changes in the

valley wind typology. Complex orography makes each valley to develop specific features as illustrated by hodographs. The wind reversal is found to be much more sudden in the Maurienne valley than in the Chamonix valley.

The TAF variability may be used to assess the differences between the local atmospheric dynamics in the two valleys. The TAF in the Maurienne valley increases from the mouth to the upper end of the valley resulting in a flow acceleration during daytime. It is nearly constant with height close to the mouth of the valley and its variability along the valley axis is in the order of 30 % from the ground surface up to the mountain ridges. In the Chamonix valley this variability is less pronounced and peaks around 25 % only near the valley floor. In addition the average TAF is about 30 % larger in the Maurienne valley than in the Chamonix valley resulting in a faster inversion breakup.

- What are the main and specific features of the boundary layer in both valleys, especially during daytime?

A fraction of the incoming radiation received on the valley unfolded surface is converted to sensible heat flux. Sensible heat flux generates the development of a CBL over the ground surface which grows up to approximately the altitude of the surrounding moun-

tains in the afternoon. The structure and evolution of the mixed layer for these days were basically similar. In the Chamonix valley convergence effects intensify the stable descending flow and delay the erosion of the stable core by the growing CBL. This interaction produces a complex boundary layer structure during the morning and evening transition periods particularly at the tethered balloon site.

- How does the local meteorology induced by complex terrain play a part in the evolution of pollutants in both valleys?

The vertical ozone distribution derived from tethered sonde measurements is strongly influenced by the diurnal evolution of the valley wind system and the boundary layer structure. During daytime the convective activity produces a rather uniform vertical distribution of O_3 concentration through the whole CBL depth. At night the NBL develops from the valley floor in response to the cooling of the ground surface. The stable stratification associated with the NBL confines surface-based pollutants. Therefore the ozone depletion due to titrating effects of NO emissions and dry deposition is limited to the lowest few hundred meters. After sunrise downward mixing of ozone from the RL and photochemical ozone formation supply the growing CBL.

These measurements have provided a useful data set to study atmospheric dynamics in complex terrain. This limited data set turned out to be efficient in characterizing clear days. The comprehension of the dynamics of the Chamonix and the Maurienne valleys enables us to extend the conclusions beyond the conditions of the intensive observation periods. Vertical exchange processes coupling the boundary layer with the air aloft are essential for air quality prediction. These processes driving the mixing ability of the air mass will be subject to further investigation. Numerical simulations could be a useful tool to refine and expand the observational investigations.

Acknowledgements

The research has been supported by the Rhône-Alpes Region, the Agency for Environment and Energy Management (ADEME), the Ministry of Equipment, Transport and Housing (METL) and the Ministry for Ecology and the Durable Development (MEDD). We are grateful to Guillaume Brulfert, Eric Chaxel and Rémi Dallmayr for assistance with tetheronde operations. We thank Bruno Bénech and Bernard Campistron for providing us with the tetheronde acquisition system and the radar postprocessing tool. We also thank Pascal Perros from the

Laboratoire Interuniversitaire des Systèmes Atmosphériques (LISA) for making available data collected in *Argentière*. Finally we are thankful to two anonymous referees for their suggestions and valuable comments on the paper.

References

- Angevine, W. M., A. B. White, and S. K. Avery: 1994, 'Boundary-layer depth and entrainment zone characterization with a boundary-layer profiler'. *Boundary-Layer Meteorol.* **68**, 375–385.
- Banta, R. M., P. B. Shepson, J. W. Bottenheim, K. G. Anlauf, H. A. Wiebe, A. Gallant, T. Biesenthal, L. D. Olivier, C. J. Zhu, I. G. McKendry, and D. G. Steyn: 1997, 'Nocturnal cleansing flows in a tributary valley'. *Atm. Environ.* **31**, 2147–2162.
- Brulfert, G., C. Chemel, E. Chaxel, and J. P. Chollet: 2005a, 'Modelling photochemistry in alpine valleys'. *Atmos. Chem. Phys.* **5**, 2341–2355.
- Brulfert, G., J. P. Chollet, B. Jouve, and H. Villard: 2005b, 'Atmospheric emission inventory of the Maurienne valley for an atmospheric numerical model'. *Sci. Tot. Env.* In Press.
- Caughey, S. J., J. C. Wyngaard, and J. C. Kaimal: 1979, 'Turbulence in the evolving stable boundary layer'. *J. Atm. Sci.* **36**, 1041–1052.
- Clements, W. E., J. A. Archuleta, and D. E. Hoard: 1989, 'Mean structure of the nocturnal drainage flow in a deep valley'. *J. Appl. Meteor.* **28**, 457–462.

- Corsmeier, U., N. Kalthoff, O. Kolle, M. Kotzian, and F. Fiedler: 1997, 'Ozone concentration jump in the stable nocturnal boundary layer during a LLJ-event'. *Atm. Environ.* **31**, 1977–1989.
- Coulter, R. L.: 1979, 'A comparison of three methods for measuring mixing-layer height'. *J. Appl. Meteor.* **18**, 1495–1499.
- Doran, J. C., T. W. Horst, and C. D. Whiteman: 1990, 'The development and structure of nocturnal slope winds in a simple valley'. *Boundary-Layer Meteorol.* **52**, 41–68.
- Fairfall, C. W.: 1991, 'The humidity and temperature sensitivity of clear-air radars in the convective boundary layer'. *J. Appl. Meteor.* **30**, 1064–1074.
- Heffter, J. L.: 1980, 'Transport layer depth calculations'. In: *Proc. of the 2nd Joint Conference on Applications of Air Pollution Modelling*. New Orleans, LA, USA, American Meteorological Society, 45 Beacon St., Boston, MA, USA, pp. 787–791.
- Helmis, C. G., D. N. Asimakopoulos, and D. G. Deligiorgi: 1990, 'Some observations on the destruction of the morning temperature inversions in a large and broad mountain valley'. *J. Appl. Meteor.* **29**, 396–400.
- Heo, B. H., S. Jacoby-Koaly, K. E. Kim, B. Campistron, B. Bénech, and E. S. Sung: 2003, 'Use of the Doppler spectral width to improve the estimation of the convective boundary layer height from UHF wind profiler observations'. *J. Atmos. Oceanic Technol.* **20**, 408–424.
- Jacoby-Koaly, S., B. Campistron, S. Bernard, B. Bénech, F. Arduin-Girard, J. Dessens, E. Dupont, and B. Carissimo: 2002, 'Turbulent dissipation rate in the boundary layer via UHF wind profiler Doppler spectral width measurements'. *Boundary-Layer Meteorol.* **103**, 361–389.
- Jaffrezo, J. L., A. Albinet, G. Aymoz, J. L. Besombes, B. Bonsang, G. Brulfert, D. Chapuis, P. Chazette, C. Chemel, J. P. Chollet, A. Colomb, P. Couvert, J.

- Cozic, E. Fréjafon, S. Geffroy, R. Greenwald, V. Jacob, C. Jambert, B. Jouve, E. Leoz-Garziandia, N. Marchand, P. Masclet, P. E. Perros, J. Rimetz, and H. Villard: 2005, 'The program POVA ('Pollution des Vallées Alpines'): general presentation and some highlights'. Submitted to *Atmos. Chem. Phys. Discussion*.
- Kaimal, J. C., N. L. Abshire, R. B. Chadwick, M. T. Decker, W. H. Hooke, R. A. Kropfli, W. D. Neff, F. Pasqualucci, and P. H. Hildebrand: 1982, 'Estimating the depth of the daytime convective boundary layer'. *J. Appl. Meteor.* **21**, 1123–1129.
- Marsik, F. J., K. W. Fischer, T. D. McDonald, and P. J. Samson: 1995, 'Comparison of methods for estimating mixing height used during the 1992 Atlanta Field Intensive'. *J. Appl. Meteor.* **34**, 1802–1814.
- Müller, H. and C. D. Whiteman: 1988, 'Breakup of a nocturnal temperature inversion in the Dischma Valley during DISKUS'. *J. Climate Appl. Meteor.* **27**, 188–194.
- Ottersten, H.: 1969, 'Atmospheric structure and radar backscattering in clear air'. *Radio Science* **4**, 1179–1193.
- Piringer, M., K. Baumann, and M. Langer: 1998, 'Summertime mixing heights at Vienna, Austria, estimated from vertical soundings and by a numerical model'. *Boundary-Layer Meteorol.* **89**, 24–45.
- Rampanelli, G. and D. Zardi: 2004, 'A method to determine the capping inversion of the convective boundary layer'. *J. Appl. Meteor.* **43**, 925–933.
- Sakiyama, S. K.: 1990, 'Drainage flow characteristics and inversion breakup in two Alberta mountain valleys'. *J. Appl. Meteor.* **29**, 1015–1030.
- Seibert, P., F. Beyrich, S. E. Gryning, S. Joffre, A. Rasmussen, and P. Tercier: 2000, 'Review and intercomparison of operational methods for the determination of the mixing height'. *Atm. Environ.* **34**, 1001–1027.

- Stewart, J. Q., C. D. Whiteman, W. J. Steenburgh, and X. Bian: 2002, 'A climatological study of thermally driven wind systems of the U.S. Intermountain West'. *Bull. Am. Met. Soc.* **84**, 699–708.
- Stull, R. B.: 1991, 'Static stability – An update'. *Bull. Am. Met. Soc.* **72**, 1521–1529.
- Weill, A., C. Klapisz, B. Strauss, F. Baudin, C. Jaupart, P. van Grunderbeek, and J. P. Goutorbe: 1980, 'Measuring heat flux and structure functions of temperature fluctuations with an acoustic Doppler sodar'. *J. Appl. Meteor.* **19**, 199–205.
- Whiteman, C. D.: 1982, 'Breakup of temperature inversions in deep mountain valleys: Part I. Observations'. *J. Appl. Meteor.* **21**, 270–289.
- Whiteman, C. D.: 1986, 'Temperature inversion buildup in Colorado's Eagle valley'. *Met. Atm. Phys.* **35**, 220–226.
- Whiteman, C. D.: 1990, 'Observations of thermally developed wind systems in mountainous terrain'. In: W. Blumen (ed.): *Atmospheric processes over complex terrain*, Vol. 23, no. 45 of *Meteorological Monographs*. American Meteorological Society, 45 Beacon St., Boston, MA, USA, Chapt. 2, pp. 5–42.
- Whiteman, C. D. and T. B. McKee: 1982, 'Breakup of temperature inversions in deep mountain valleys: Part II. Thermodynamic model'. *J. Appl. Meteor.* **21**, 290–302.

List of Figures

- 1 Vertical virtual potential temperature profile and analysis of non-local static stability. Tethered balloon data, *Les Praz de Chamonix* in the Chamonix valley, July 8, 2003 at 0617 UTC 38
- 2 Overview of a part of the Alps with location of the Chamonix (site **A**) and the Maurienne (site **B**) valleys in UTM coordinate system, zone 32. Attached grey scale indicates altitude in meters above mean sea level (a.m.s.l.) 39
- 3 Time-height cross section of refractive index structure parameter C_n^2 (**a**) and turbulent kinetic energy dissipation rate ϵ (**b**) for July 8, 2003 at *Le Clos de l'Ours* in the Chamonix valley. CBL depths were superimposed on C_n^2 contours: \circ derived from the maximum backscatter intensity method combined with the variance of vertical air velocity σ_w^2 and \star estimated using tethered profiles 40
- 4 Wind structure pattern evolution. Tethered balloon data, *Les Praz de Chamonix* in the Chamonix valley, July 8, 2003 41

	Observations of the daytime boundary layer in deep alpine valleys	35
5	Time-height cross sections of horizontal wind speed (a) and direction (b) for July 8, 2003 at <i>Le Clos de l'Ours</i> in the Chamonix valley	42
6	Potential temperature profile evolution. Tethered bal- loon data, <i>Les Praz de Chamonix</i> in the Chamonix val- ley, July 8, 2003. See Figure 4 for corresponding times (only ascending soundings U# are displayed in the morn- ing)	43
7	Cross-section along the Chamonix valley axis	44
8	Ozone concentration profile evolution. Tethered balloon data, <i>Les Praz de Chamonix</i> in the Chamonix valley, July 8, 2003. See Figure 4 for corresponding times (only ascending soundings U# are displayed in the morning)	45
9	Time series of ozone concentration in <i>Le Clos de l'Ours</i> (a) and NO_x/NO_y ratio in <i>Argentière</i> (b) . Ground mon- itoring station data in the Chamonix valley, July 8-9, 2003	46
10	Wind structure pattern evolution. Tethered balloon data, <i>Modane</i> in the Maurienne valley, June 29, 2003	47

	Observations of the daytime boundary layer in deep alpine valleys	36
11	Hodographs: (a) <i>Modane</i> ground monitoring station in the Maurienne valley on June 29, 2003 (b) <i>Argentière</i> ground monitoring station in the Chamonix valley on July 8, 2003	48
12	Representative parts used for TAF computations: (a) Chamonix valley (b) Maurienne valley	49
13	TAF as a function of nondimensional height for each part of both valleys (\circ part 1, \square part 2, \triangle part 3): (a) Chamonix valley (b) Maurienne valley	50

Tables

Table I. Characteristics of the UHF radar wind profiler used in the POVA experiment

Parameters	Characteristic value
Transmitter	
frequency	1238 MHz
wavelength	24.2 cm
peak power	4 kW
pulse length	150 m
pulse repetition frequency	20000 Hz
one-way beam width	8.5°
Antenna	
type	3-panel array
one vertical beam (elevation angle)	90°
two oblique beams (off-zenith angle)	17°
antenna area	2 m ²
Receiver	
number of FFT points	128
number of incoherent integrations	10
number of coherent integrations	100
Inter Pulse Period	30 μ s
number of gate	50
range resolution	80 m
maximum unambiguity range	6 km
velocity resolution	0.1 m s ⁻¹
maximum unambiguity velocity	6 m s ⁻¹
minimum detectable signal	18.8 dBZ

Figures

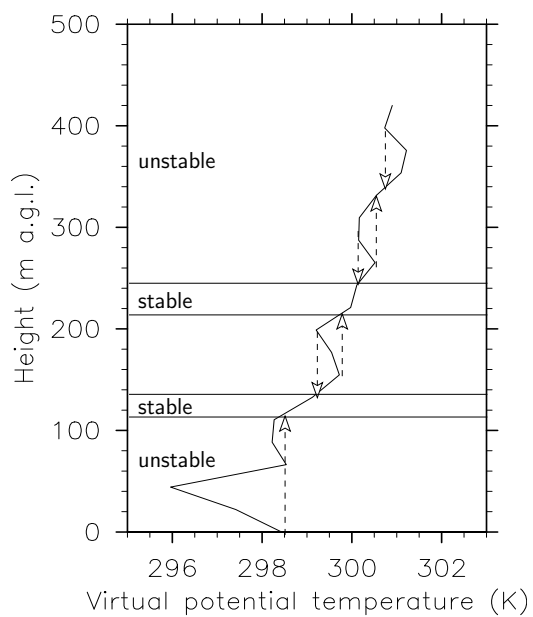


Figure 1. Vertical virtual potential temperature profile and analysis of non-local static stability. Tethered balloon data, *Les Praz de Chamonix* in the Chamonix valley, July 8, 2003 at 0617 UTC

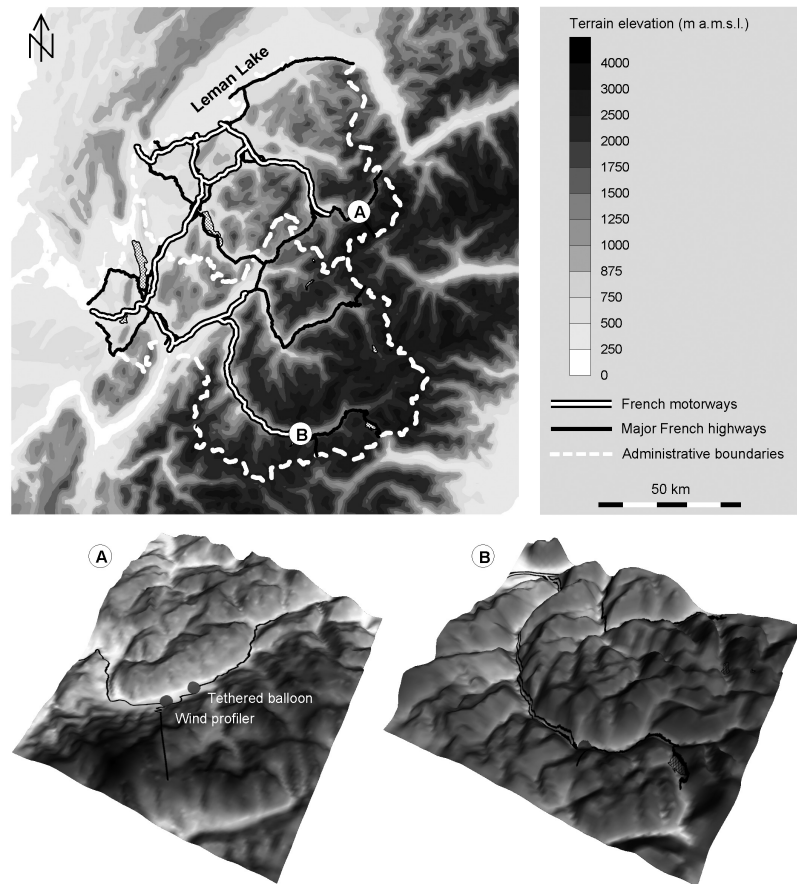


Figure 2. Overview of a part of the Alps with location of the Chamonix (site **A**) and the Maurienne (site **B**) valleys in UTM coordinate system, zone 32. Attached grey scale indicates altitude in meters above mean sea level (a.m.s.l.)

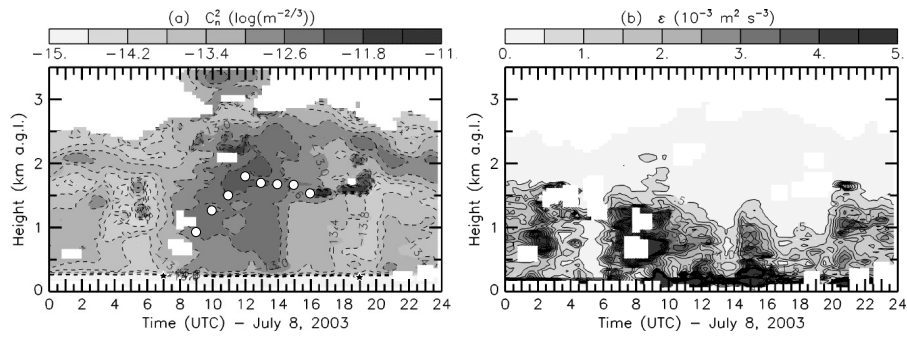


Figure 3. Time-height cross section of refractive index structure parameter C_n^2 (a) and turbulent kinetic energy dissipation rate ϵ (b) for July 8, 2003 at *Le Clos de l'Ours* in the Chamonix valley. CBL depths were superimposed on C_n^2 contours: \circ derived from the maximum backscatter intensity method combined with the variance of vertical air velocity σ_w^2 and \star estimated using tethered sonde profiles

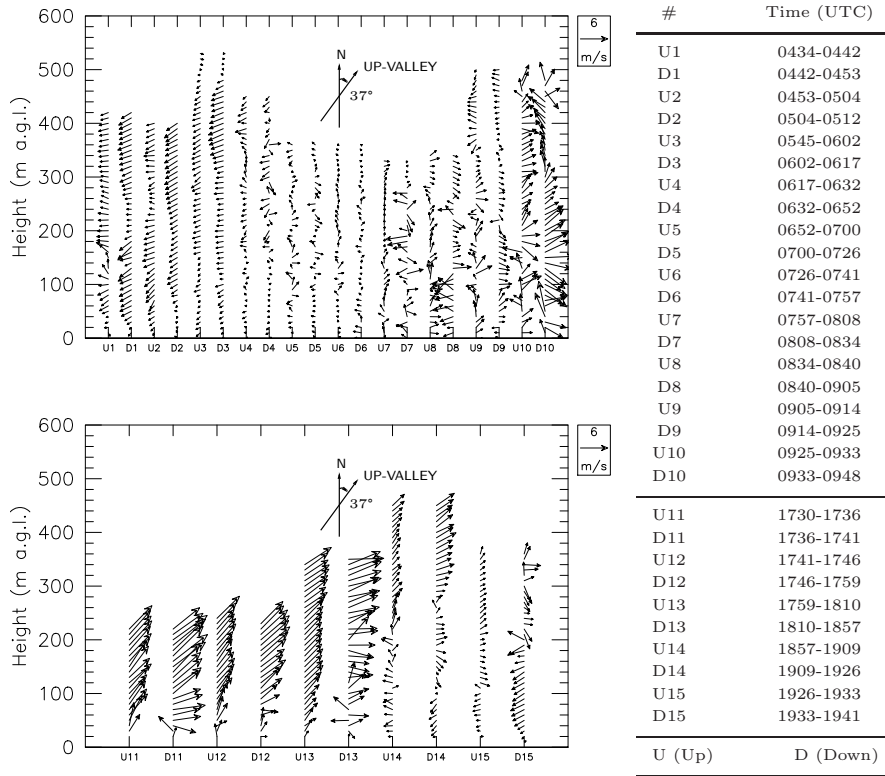


Figure 4. Wind structure pattern evolution. Tethered balloon data, *Les Praz de Chamonix* in the Chamonix valley, July 8, 2003

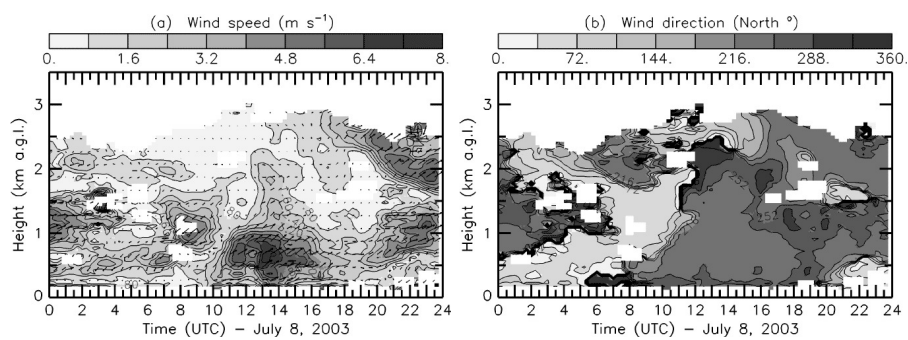


Figure 5. Time-height cross sections of horizontal wind speed (a) and direction (b) for July 8, 2003 at *Le Clos de l'Ours* in the Chamonix valley

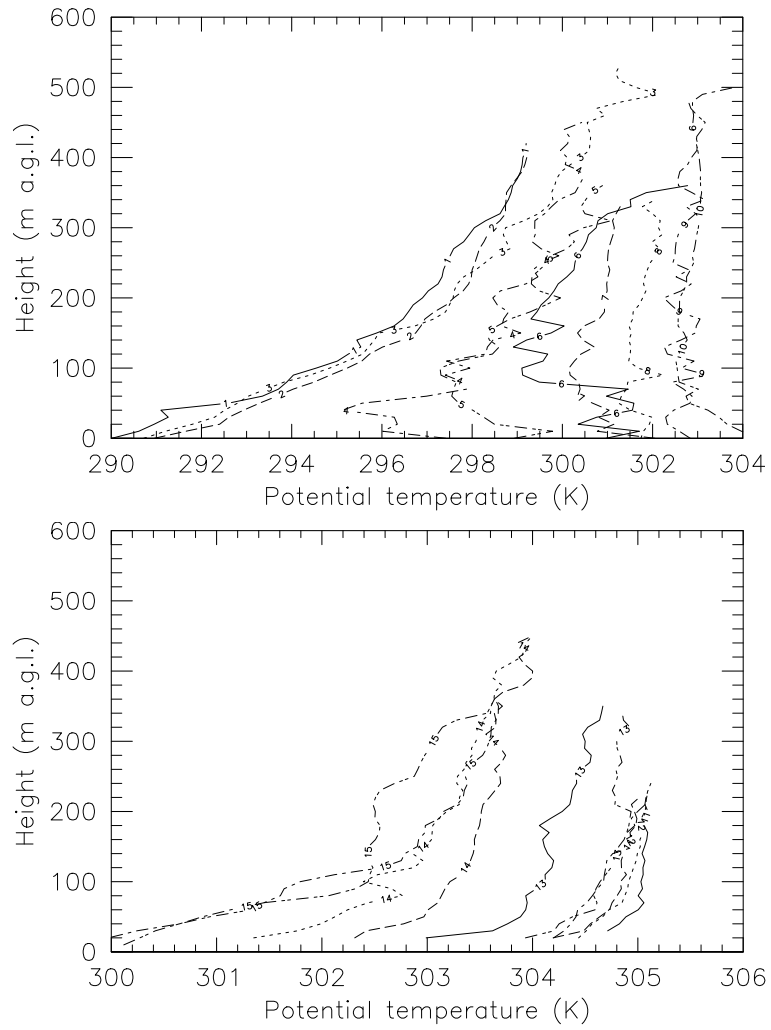


Figure 6. Potential temperature profile evolution. Tethered balloon data, *Les Praz de Chamonix* in the Chamonix valley, July 8, 2003. See Figure 4 for corresponding times (only ascending soundings U# are displayed in the morning)

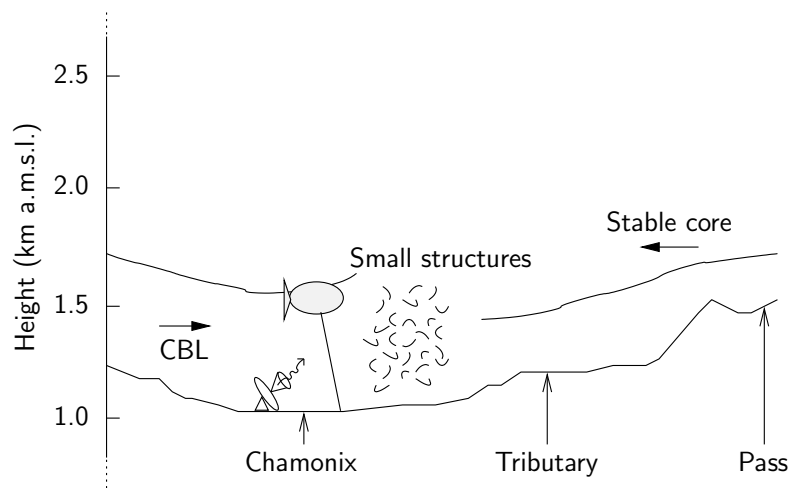


Figure 7. Cross-section along the Chamonix valley axis

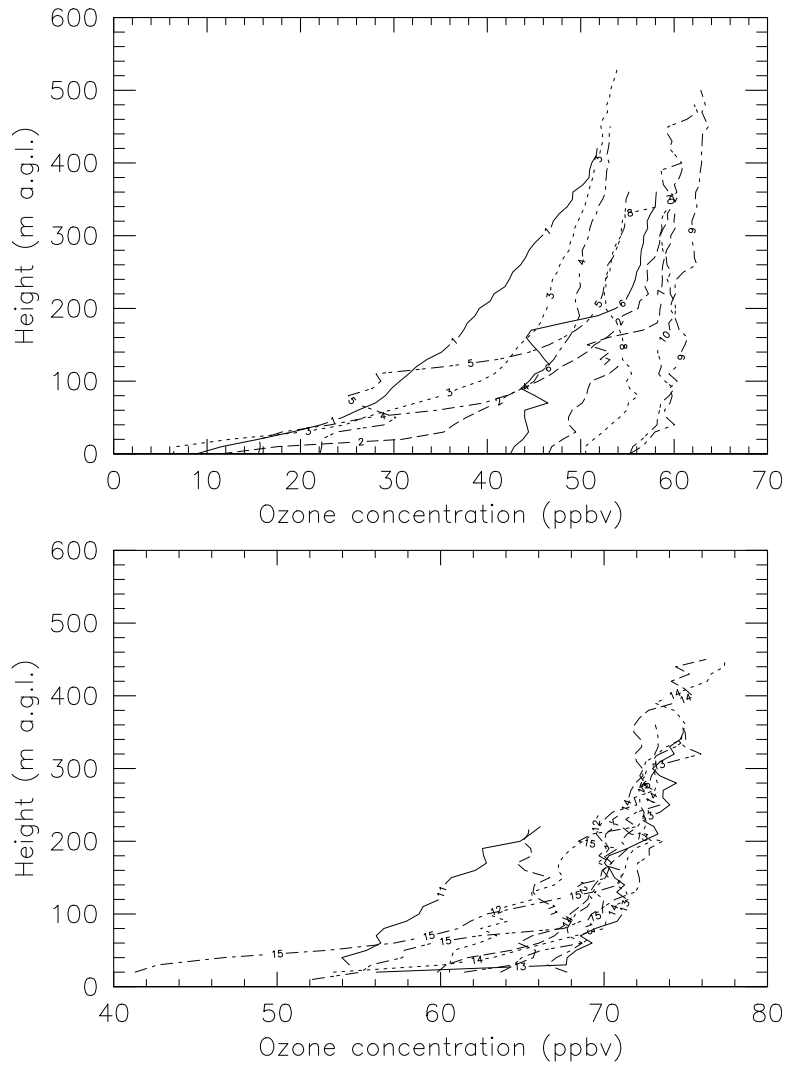


Figure 8. Ozone concentration profile evolution. Tethered balloon data, *Les Praz de Chamonix* in the Chamonix valley, July 8, 2003. See Figure 4 for corresponding times (only ascending soundings U# are displayed in the morning)

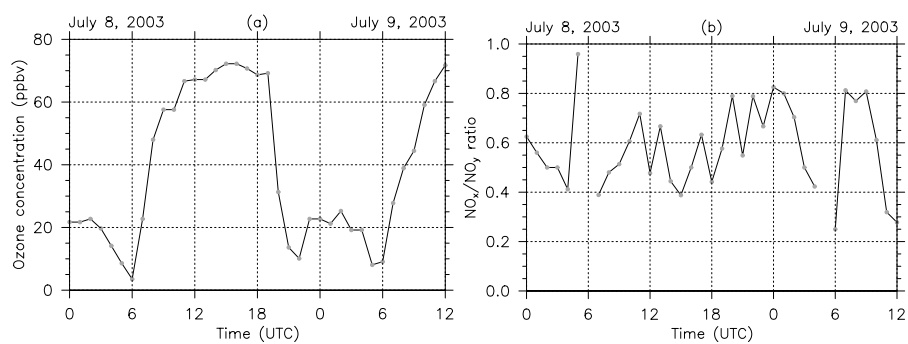


Figure 9. Time series of ozone concentration in *Le Clos de l'Ours* (a) and NO_x/NO_y ratio in *Argentière* (b). Ground monitoring station data in the ChamoniX valley, July 8-9, 2003

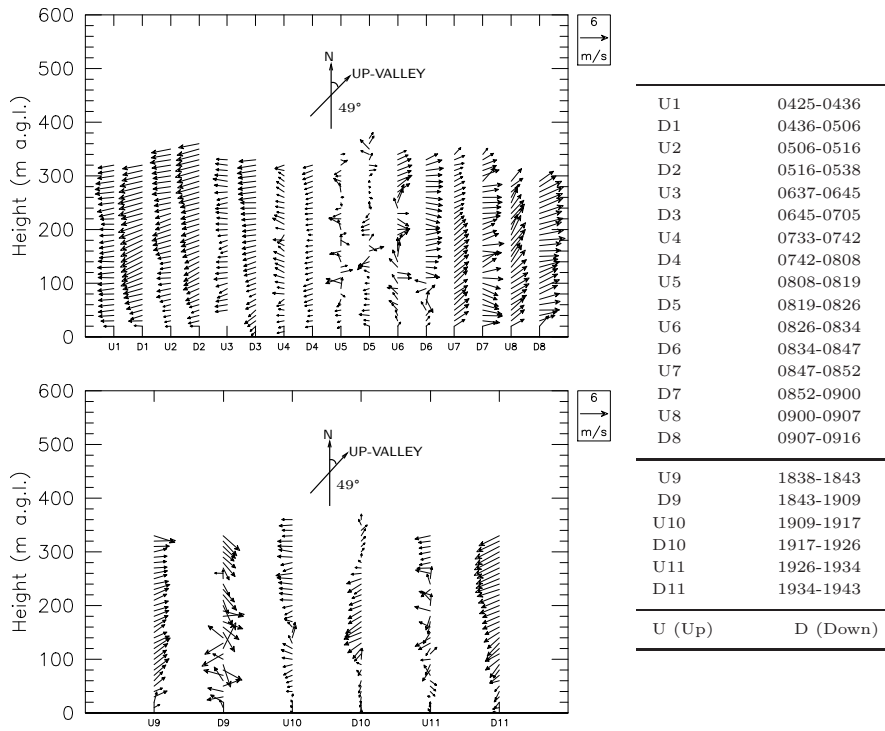


Figure 10. Wind structure pattern evolution. Tethered balloon data, Modane in the Maurienne valley, June 29, 2003

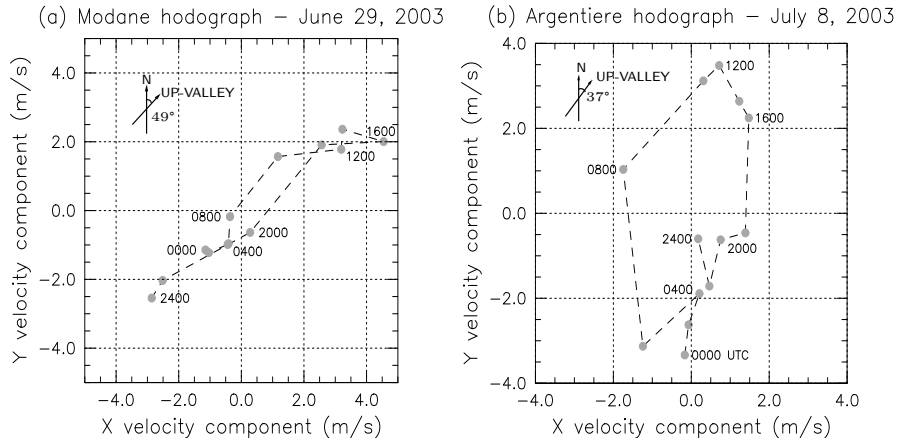


Figure 11. Hodographs: (a) *Modane* ground monitoring station in the Maurienne valley on June 29, 2003 (b) *Argentière* ground monitoring station in the Chamonix valley on July 8, 2003

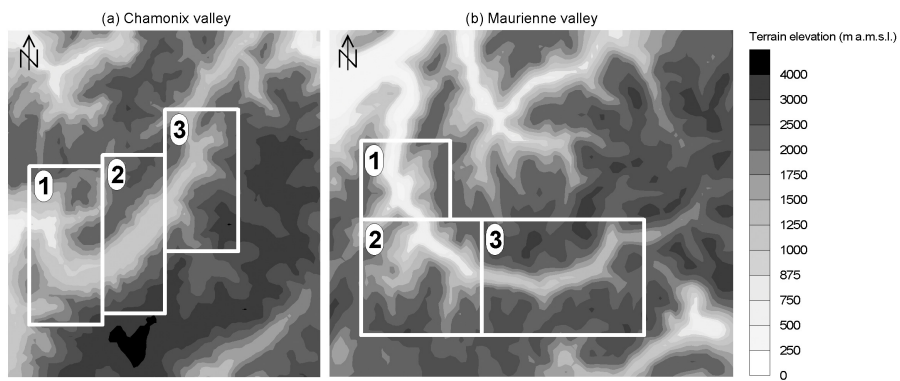


Figure 12. Representative parts used for TAF computations: (a) Chamonix valley
(b) Maurienne valley

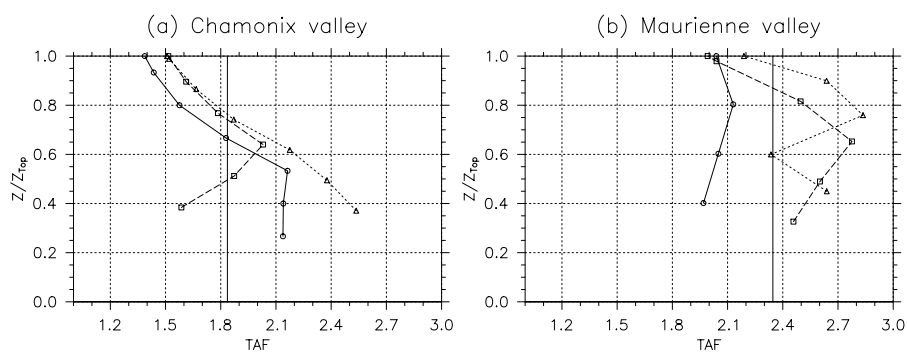


Figure 13. TAF as a function of nondimensional height for each part of both valleys (○ part 1, □ part 2, △ part 3): (a) Chamonix valley (b) Maurienne valley